Effect of Sunlight Polarization on the Absorption Efficiency of V-shaped Organic Solar Cells

Kyungnam Kang and Jungho Kim*

Department of Information Display and Advanced Display Research Center, Kyung Hee University, Seoul 130-701, Korea

We numerically investigate the effect of sunlight polarization on the absorption efficiency of V-shaped organic solar cells (VOSCs) using the finite element method (FEM). The spectral distribution of absorbance and the spatial distribution of power dissipation are calculated as a function of the folding angle for *s*- and *p*-polarized light. The absorption enhancement caused by the light-trapping effect was more pronounced for *s*-polarized light at folding angles smaller than 20°, where *s*-polarized light has a relatively larger reflectance than *p*-polarized light. On the other hand, the absorption efficiency for *p*-polarized light is relatively larger for folding angles larger than 20°, where the smaller reflectance at the interface of the VOSC is more important in obtaining high absorption efficiency.

I. INTRODUCTION

Organic solar cells (OSCs) have drawn great attention as a promising renewable energy generator due to their potential for cheap processing on large areas, mechanical flexibility, and light weight [1, 2]. In spite of much research effort, the power conversion efficiency (PCE) of commercial OSCs is still lacking, compared to that of silicon-based inorganic solar cells [3]. The main problem is that most organic materials have a serious limitation for the probability that an absorbed photon contributes to photocurrent, known as the internal quantum efficiency (IQE). The active layer must be kept thick enough to absorb most incident photons, which results in increasing the probability for charge recombination, which decreases the IQE. The trade-off between optical absorption and charge carrier transport should be carefully considered in the determination of device thickness in OSCs [4, 5].

Recently, various light-trapping schemes such as metal gratings [6], buried nanoelectrodes [7], scattering elements [8], and multiple-reflection structures [9] have been proposed to enhance light absorption in OSCs without thickening the active layer. Among them, V-shaped organic solar cells

(VOSCs) have shown a double enhancement of PCE compared to planar cells [9]. Part of the incident light that is not absorbed by one arm is reflected onto the other arm, which gives a greater chance for it to be absorbed in the active layer and increases the PCE due to the light-trapping effect [10]. Moreover, VOSCs can be applicable to tandem or multiple-bandgap OSCs, where different bandgap materials are used on each arm of a V-shaped substrate to broaden the absorption spectrum [11, 12].

Optical modeling based on the finite element method (FEM) has been performed to investigate the optical behavior of VOSCs with respect to layer thickness and folding angle [11, 12]. Polarization of sunlight should be considered in the optical modeling of VOSCs because *s*- and *p*-polarized light in oblique incidence will have different reflectance at the interface of the V-shaped arm with a certain folding angle. However, the effect of light polarization on the absorption efficiency has not yet been fully investigated in the optical modeling of VOSCs.

In this paper, we present comprehensive optical modeling results based on the FEM, focusing on the dependence of light polarization on the absorption behavior of VOSCs. The spectral distribution of absorbance and the spatial

---

*Corresponding author: junghokim@khu.ac.kr

distribution of power dissipation are each calculated as a function of the folding angle for *s*- and *p*-polarized light. We investigate how the absorption efficiency of the VOSC is affected by light polarization and folding angles.

II. SIMULATION MODEL

The direction of the electric field oscillations is composed of *s*- and *p*-polarizations that are orthogonal to or parallel to the plane of incidence, respectively. We set the arm length of the VOSC to be l = 5 μm and two arms are tilted to the normal incident light with a folding angle of α. As shown in the inset, the OSC consists of indium tin oxide (ITO) (100 nm) as an anode, poly(3,4-ethylenedioxy-thiophene):poly(styrene sulfonate) (PEDOT:PSS) (40 nm) as a hole transporting layer, poly(3-hexylthiophene):[6,6]-phenyl C61-butyric acid methyl ester (P3HT:PCBM) (100 nm) as an active layer, and aluminum (Al) (100 nm) as a cathode. The value of the complex refractive index ($\tilde{n} = n + i\kappa$) of each layer is measured via ellipsometry in the wavelength range from 300 to 900 nm [13].

For planar OSCs, the transfer matrix method (TMM) described by 2×2 matrices has been widely used to calculate the absorption behavior for both *s*- and *p*-polarized light [13-20]. However, this method is not applicable to nonplanar structures such as textured gratings and folded structures. Thus, the optical modeling of VOSCs is performed based on two-dimensional FEM calculations, where the commercial software COMSOL MULTIPHYSICS is used as the FEM solver [21]. To investigate the polarization-dependent absorption behavior of the VOSC, the spectral distribution of absorbance and the spatial distribution of power dissipation are calculated with respect to the folding angle for *s*- and *p*-polarized light.

The time-average power dissipation per volume, for one wavelength, is defined as

$$Q(\lambda) = \langle -\nabla \cdot \mathbf{S} \rangle, \tag{1}$$

where λ is the wavelength and the unit of $Q(\lambda)$ is W/m^3. The Poynting vector $\mathbf{S}$ is given by

$$\mathbf{S} = \frac{1}{2}\mathbf{E} \times \mathbf{H}^*, \tag{2}$$

where $\mathbf{E}$ is the electric field amplitude vector and $\mathbf{H}^*$ is the complex conjugate of the magnetic field amplitude vector. The absorbance $A(\lambda)$ is obtained by integrating the power dissipation at one wavelength over the whole active layer

$$A(\lambda) = \frac{1}{S_0} \int_{active} Q(\lambda, r) dr, \tag{3}$$

where S_0 is the incident optical power from the air on the uppermost boundary, and r is the x-y coordinate on the two-dimensional plane. Finally, the total absorbance A^{tot} is obtained by averaging the absorbance $A(\lambda)$ for the whole wavelength range from 300 to 900 nm. For solar cell applications, the input light should be the AM 1.5 sunlight model instead of the normalized power. Therefore, the solar absorbance A^{solar} considering AM 1.5 sunlight input is given by

$$A^{solar} = \frac{1}{P_0} \iint_{active} P_{solar}(\lambda) Q(\lambda, r) dr d\lambda, \tag{4}$$

where P_0 is the incident optical power summing the spectral irradiance of the AM 1.5 sunlight over the whole wavelength range, and $P_{solar}(\lambda)$ is the spectral irradiance of the AM 1.5 sunlight at one wavelength.

III. CALCULATION RESULTS

Because the number of the multiple reflections between two arms of the VOSC increases at smaller folding angles,
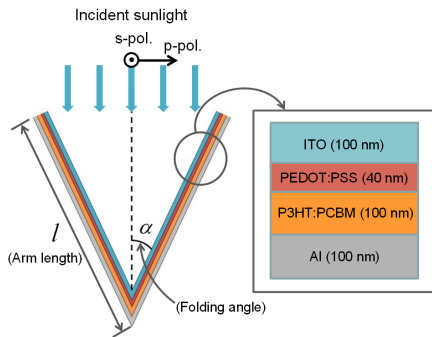

FIG. 1. Schematic diagram of the device structure along with material's composition and thickness of each layer. The plane wave is assumed to enter the OSC structure from the air at the uppermost boundary. The direction of the electric field oscillations is perpendicular (*s*-polarization) or parallel (*p*-polarization) to the incident plane. Two arms of the VOSC are tilted to the normal incident light with a folding angle of α.
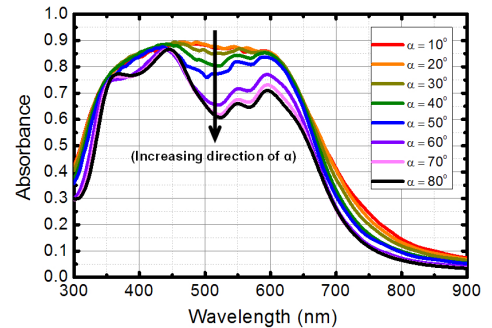

FIG. 2. Calculated absorptance spectra in the active layer (P3HT:PCBM) of the VSOC for various folding angles. As the folding angle decreases, the absorptance increases and becomes saturated.
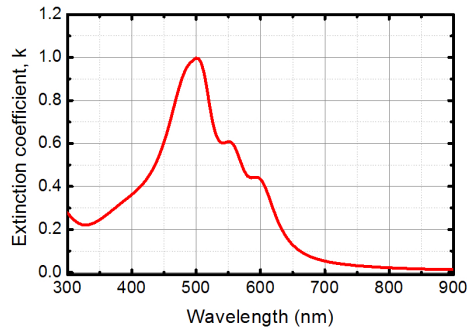
FIG. 3. The extinction coefficient spectra of the active layer (P3HT : PCBM), which has the peak value at the wavelength of 500 nm and shows the ripple between 500 and 600 nm.

the light-trapping effect is more prominent for smaller folding angles [10]. Thus, the overall absorbance in Fig. 2 increases as the folding angle decreases and becomes saturated at an angle of 10°. The absorbance enhancement caused by the folded arms is more visible in the wavelength range of 450-600 nm, due to the significant absorption coefficient of the P3HT:PCBM active layer around 500 nm, as shown in Fig. 3. The small ripples in the absorbance spectra between 500 and 600 nm are ascribed to the ripples in the extinction coefficient of the P3HT:PCBM active layer, shown in Fig. 3.
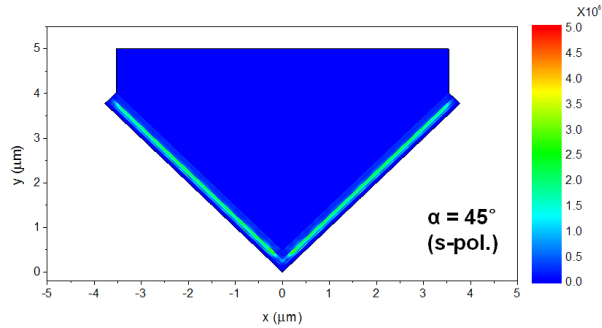
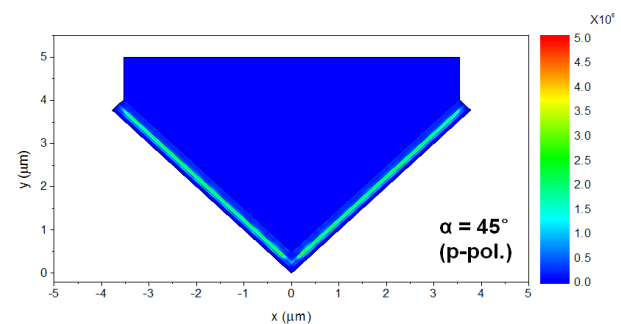Figures 4 and 5 show the spatial distributions of the power dissipation in the VOSC at folding angles of 20°,
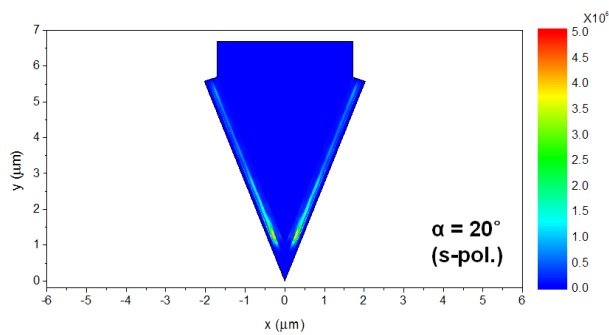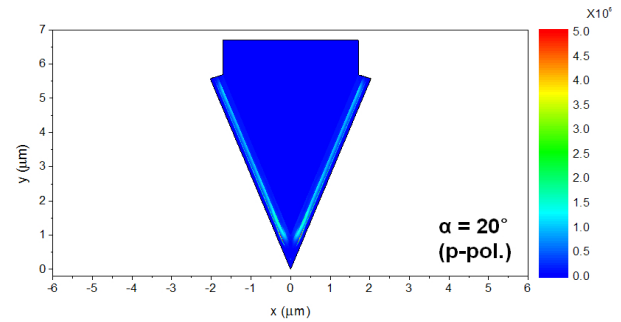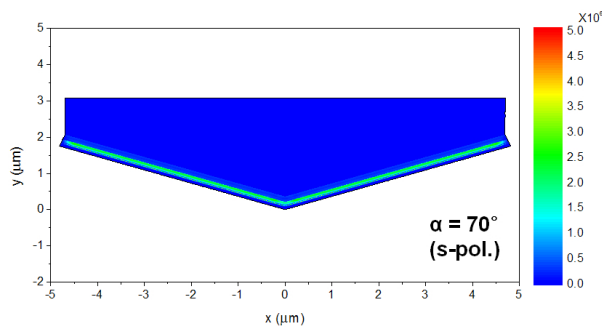

FIG. 4. The spatial distribution of the power dissipation in the VOSC at the folding angle of $\alpha =$ (a) 20°, (b) 45°, and (c) 70° for s-polarized light. The spatial distribution of the power dissipation is obtained by taking the summation over the whole wavelength range.
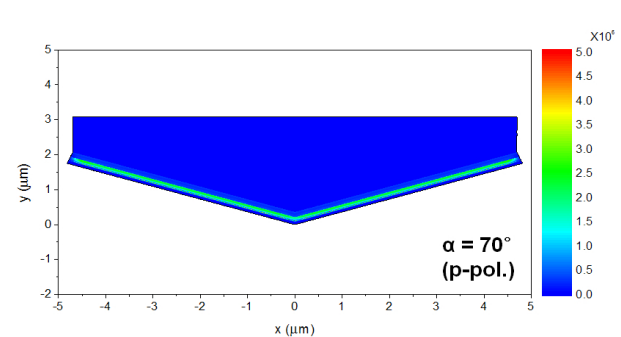

FIG. 5. The spatial distribution of the power dissipation in the VOSC at the folding angle of $\alpha =$ (a) 20°, (b) 45°, and (c) 70° for p-polarized light. The spatial distribution of the power dissipation is obtained by taking the summation over the whole wavelength range.

45°, and 70° for *s*- and *p*-polarized light, respectively. The spatial distribution of the power dissipation is obtained by summing over the whole wavelength range. At the folding angle of $\alpha = 20°$, the power dissipation is more concentrated in the bottom of the V-shaped structure for *s*-polarized light, while the power dissipation is relatively uniformly distributed all around the arm for *p*-polarized light. On the other hand, the spatial distributions of the power distribution are very uniform for both polarizations at the larger folding angles of $\alpha = 45°$ and $\alpha = 70°$. This behavior can be explained by the polarization-dependent reflectance spectra at the interface of the VOSC, as discussed below.

The reflectance at the planar OSC structure shown in the inset of Fig. 1 is calculated based on the TMM. For the folding angles $\alpha = 20°$, 45°, and 70°, the corresponding incidence angles at the interface of the VOSC $\theta = 70°$, 45°, and 20°, in terms of the oblique incidence for planar solar cells. At the small folding angle $\alpha = 20°$ ($\theta = 70°$),

the reflectance for *s*-polarized light is much larger across almost all of the wavelength range than that for *p*-polarized light. Thus, *s*-polarized light experiences more multiple reflections between two arms and has more concentrated light absorption near the bottom of the V-shaped structure than *p*-polarized light, as shown in Figs. 4(a) and 5(a). As the folding angle increases to $\alpha = 45°$ and 70°, the difference in reflectance between *s*- and *p*-polarized light becomes smaller, as in Fig. 6. In addition, the possible number of multiple reflections between the two arms becomes smaller, approaching zero as the folding angle increases [10, 11]. Therefore, the spatial distributions of the power dissipation in Fig. 4 and 5 are uniform for both polarizations at the larger folding angles of $\alpha = 45°$ and 70°.

In view of light polarization, *p*-polarized light has relatively higher absorbance than *s*-polarized light at all folding angles, which is ascribed to the lower reflectance of *p*-polarized light at the interface of the VOSC, as shown in Fig. 6.

When the folding angle is smaller than 20°, *s*-polarized light has the relatively higher total absorbance than *p*-polarized light, because the absorption enhancement due to the
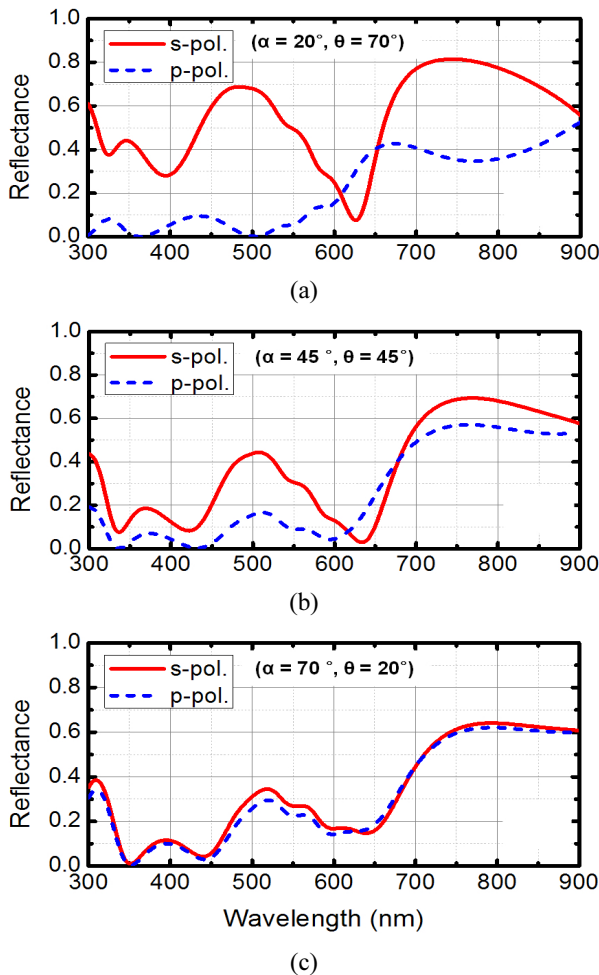
(a)

(b)

(c)

FIG. 6. Calculated reflectance spectra at the interface of the VOCS at the folding angle of $\alpha = 20°$, 45°, and 70° for *s*- and *p*-polarized light. For the folding angles of $\alpha = 20°$, 45°, and 70°, the incidence angle at the interface of the VOSC corresponds to $\theta = 70°$, 45°, and 20° in terms of the oblique incidence for planar solar cells.

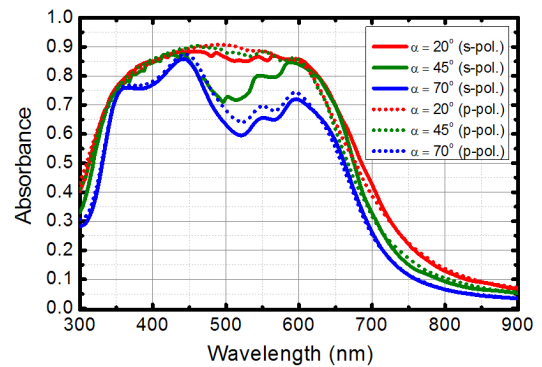FIG. 7. Calculation results of polarization-dependent absorptance spectra in the active layer of the VOSC at the folding angles of $\alpha = 20°$, 45°, and 70°. Both polarizations have relatively high absorptance at the small folding angle due to the enhanced light trapping effect.
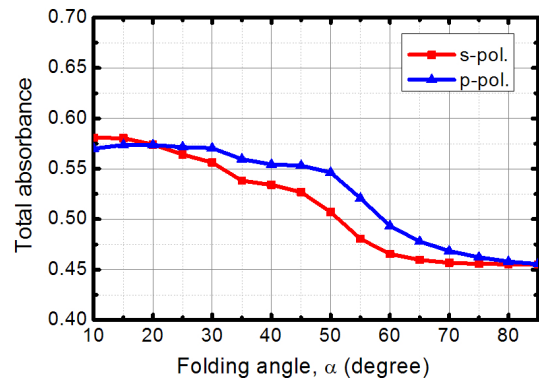
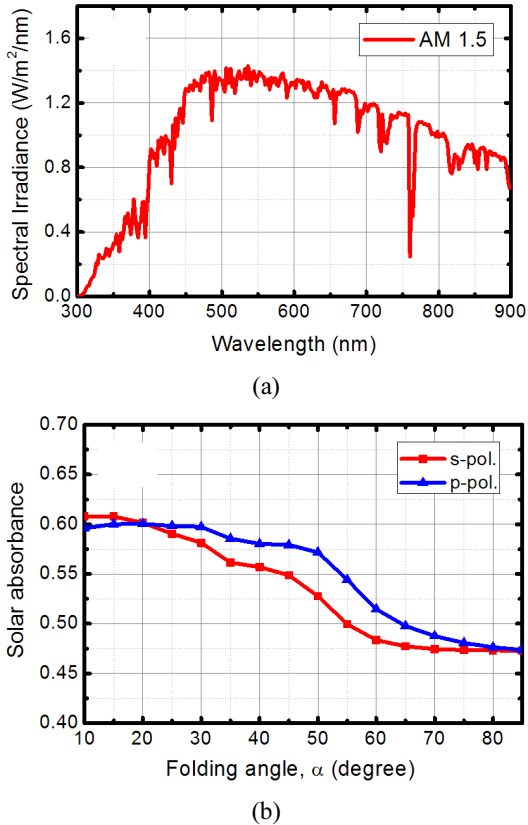FIG. 8. Calculated total absorptance of the VOCS as a function of the folding angle α for *s*- and *p*-polarized light.

(a)

(b)

FIG. 9. (a) Optical spectra of the AM 1.5 sunlight. (b) Calculated solar absorptance of the VOSC as a function of the folding angle α for s- and p-polarized light.

light-trapping effect is more significant at these folding angles. On the other hand, p-polarized light has the relatively higher total absorbance at folding angles larger than 20°, where the light-trapping effect becomes less pronounced and the smaller reflectance at the interface of the VOSC is more important in obtaining higher total absorbance.

In the realistic performance evaluation of solar cells, the optical spectrum of input light should follow the AM 1.5 sunlight model in Fig. 9(a) instead of the normalized power across the whole wavelength range. Figure 9(b) shows the calculated solar absorbance of the VOSC as a function of folding angle for s- and p-polarized light. The solar absorbance in Fig. 9(b) considering AM 1.5 sunlight is close to the total absorbance in Fig. 8, where normalized input power is used over the whole spectrum. This small difference between the total and solar absorbance of the VOSC results from the fact that the range of strong absorption for the P3HT: PCBM active layer around 500 nm matches the high spectral power of AM 1.5 sunlight.

IV. CONCLUSION

We numerically investigated the polarization-dependent absorption behavior of the VOSC with respect to the folding

angle. The absorption enhancement caused by the light-trapping effect was more prominent for s-polarized light because s-polarized light has a relatively larger reflectance than p-polarized light at smaller folding angles. On the other hand, the absorption efficiency for p-polarized light is relatively larger than for s-polarized light at folding angles larger than 20°, where the smaller reflectance at the interface of the VOSC is more important in obtaining high absorption efficiency. We expect these optical modeling results to help in designing a more efficient VOSC with higher PCE.

REFERENCES

1. K. M. Coakley and M. D. McGehee, "Conjugated polymer photovoltaic cells," Chem. Mater. **16**, 4533-4542 (2004).
2. H. Hoppe and N. S. Sariciftci, "Organic solar cells: An overview," J. Mater Res. **19**, 1924-1945 (2004).
3. C. J. Brabec, "Organic solar cells: An overview," Sol. Energy Mater. Sol. Cells **83**, 273-292 (2004).
4. P. Peumans, V. Bulović, and S. R. Forrest, "Efficient photon harvesting at high optical intensities in ultrathin organic double-heterostructure photovoltaic diodes," Appl. Phys. Lett. **76**, 2650 (2000).
5. P. Peumans, A. Yakimov, and S. R. Forrest, "Small molecular weight organic thin-film photodetectors and solar cells," J. Appl. Phys. **93**, 3693 (2003).
6. L. S. Roman, O. Inganäs, T. Granlund, T. Nyberg, M. Svensson, M. R. Andersson, and J. C. Hummelen, "Trapping light in polymer photodiodes with soft embossed gratings," Adv. Mater. **12**, 189-195 (2000).
7. M. Niggemann, M. Glatthaar, A. Gomber, A. Hinsch, and V. Wittwer, "Diffraction gratings and buried nano-electrodes -architectures for organic solar cells," Thin Solid Films **451-452**, 619-623 (2004).
8. K. Tvingstedt, M. Tormen, L. Businaro, and O. Inganäs, "Light confinement in thin film organic photovoltaic cells," Proc. SPIE **6197**, 61970C (2006).
9. K. Tvingstedt, V. Andersson, F. L. Zhang, and O. Inganäs, "Folded reflective tandem polymer solar cell doubles efficiency," Appl. Phys. Lett. **91**, 123514 (2007).
10. S.-B. Rim, S. Zhao, S. R. Scully, M. D. McGehee, and P. Peumans, "An effective light trapping configuration for thin-film solar cells," Appl. Phys. Lett. **91**, 243501 (2007).
11. V. Andersson, K. Tvingstedt, and O. Inganäs, "Optical modeling of a folded organic solar cell," J. Appl. Phys.

103, 094520 (2008).

12. B. V. Andersson, N.-K. Persson, and O. Inganäs, "Comparative study of organic thin film tandem solar cells in alternative geometries," J. Appl. Phys. **104**, 124508 (2008).

13. S. Lee, I. Jeong, H. P. Kim, S. Y. Hwang, T. J. Kim, Y. D. Kim, J. Jang, and J. Kim, "Effect of incidence angle and polarization on the optimized layer structure of organic solar cells," Sol. Energy Mater. Sol. Cells **118**, 9-17 (2013).

14. L. A. A. Pettersson, L. S. Roman, and O. Inganäs, "Modeling photocurrent action spectra of photovoltaic devices based on organic thin films," J. Appl. Phys. **86**, 487-496 (1999).

15. D. Cheyns, B. P. Rand, B. Verreet, J. Genoe, J. Poortmans, and P. Heremans, "The angular response of ultrathin film organic solar cells," Appl. Phys. Lett. **92**, 243310 (2008).

16. A. Meyer and H. Ade, "The effect of angle of incidence on the optical field distribution within thin film organic solar cells," J. Appl. Phys. **106**, 113101 (2009).

17. S. Jung, K.-Y. Kim, Y.-I. Lee, J.-H. Youn, H.-T. Moon, J. Jang, and J. Kim, "Optical modeling and analysis of organic solar cells with coherent multilayers and incoherent glass substrate using generalized transfer matrix method," Jpn. J. Appl. Phys. **50**, 122301 (2011).

18. J. Kim, S. Jung, and I. Jeong, "Optical modeling for polarization-dependent optical power dissipation of thin-film organic solar cells at oblique incidence," J. Opt. Soc. Korea **16**, 6-12 (2012).

19. S. Jung, Y.-I. Lee, J.-H. Youn, H.-T. Moon, J. Jang, and J. Kim, "Effect of the active-layer thickness on the short-circuit current analyzed using the generalized transfer matrix method," J. Inf. Display **14**, 7-11 (2013).

20. K. Kang, S. Lee, and J. Kim, "Effect of an incoherent glass substrate on the absorption efficiency of organic solar cells at oblique incidence analyzed by the transfer matrix method with a glass factor," Jpn. J. Appl. Phys. **52**, 052301 (2013).

21. COMSOL Multiphysics, Version 4.3a Comsol Inc. (2012), http://www.comsol.com.